

# RF SIMULATIONS FOR THE QWR CAVITIES OF PIAVE-ALPI

M. Comunian, A. Palmieri, F. Grespan INFN-LNL, Legnaro (PD), Italy

## Abstract

The PIAVE-ALPI linac is composed of several families of QWR cavities. In order to have a thorough description of the accelerator in terms of beam dynamics, a detailed field mapping of the accelerating cavities is necessary, including non-linear behaviour of the off-axis fields, as well as the steering and dispersion effects due to transverse components. For such a purpose, a set of RF simulation was accomplished, with the codes HFSS and COMSOL. The details about these simulations and the main outcomes and results will be described in this article.

## ALPI LAYOUT

The ALPI (Acceleratore Lineare Per Ioni) accelerator is a flexible structure for the study of heavy ion for nuclear physics which is able to deliver ions from Si to U with a final beam energy range from 6 up to 20 MeV/u. The facility consists of a series of 71 independently phased superconducting Quarter Wave Resonators (QWRs) accelerating cavities operating at two different frequencies, namely 80 and 160 MHz, (Figure 1).

The accelerating elements of the linac are the Low Beta QWRs with  $\beta_s=0.047$ ,  $\beta_s=0.055$  at 80 MHz, medium beta QWRs with  $\beta_s=0.11$ , and high beta QWRs with  $\beta_s=0.13$  at 160 MHz. [1].

## RF SIMULATIONS (COMSOL AND HFSS)

The above-mentioned structures were simulated by using the codes HFSS v.12 and COMSOL v.4 on a 64 bit machine with 64 Gb RAM. The cavity solids were imported as .sat (ACIS) files with their nominal dimensions. Both HFSS and COMSOL are finite-element codes, making use of a tetrahedral mesh structure. The number of mesh elements employed for these simulations is in the order of 700000 tetrahedra, while the memory used is in the order of 60 GByte for COMSOL and 20 GByte for HFSS respectively (Fig.1).

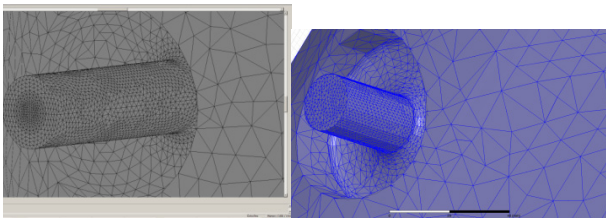


Figure 1: The details of the mesh for COMSOL (left) and HFSS (right).

In the following table the value of some significant parameters will be given for both codes, namely resonant frequencies and the value  $U/Eacc^2$  defined as

$$\frac{U}{E_{acc}^2} = \frac{1}{4} \iiint_V (\epsilon_0 |\mathbf{E}|^2 + \mu_0 |\mathbf{H}|^2) / \left( \int_{-L/2}^{L/2} |E_z(z)| dz / L \right)^2$$

As well as the TTF factor, calculated as:

$$TTF(\beta) = \int_{-L/2}^{L/2} E_z(z) \sin\left(\frac{2\pi z}{\beta\lambda}\right) dz / \int_{-L/2}^{L/2} |E_z(z)| dz$$

The line integrals being calculated on the cavity axis and L being the cavity length.

Table 1: Main parameters for the four families of cavities

QWR Type	0.047	0.052	0.11	0.13
$f_{HFSS}$ [MHz]	79.765	79.805	159.566	159.531
$f_{COMSOL}$ [MHz]	79.734	79.743	159.213	160.665
$U/Eacc^2$ (HFSS) [mJ/(MV/m) <sup>2</sup> ]	98.4	98.1	52.4	55.0
$U/Eacc^2$ (COMSOL) [mJ/(MV/m) <sup>2</sup> ]	98.9	98.6	53.0	54.7
$\beta_{opt}$ (HFSS)	0.048	0.057	0.109	0.128
$\beta_{opt}$ (COMSOL)	0.048	0.057	0.109	0.128
TTF ( $\beta_{opt}$ ) (HFSS)	0.87	0.90	0.90	0.89
TTF ( $\beta_{opt}$ ) (COMSOL)	0.87	0.90	0.90	0.89

In the following Figure 2 the simulation outputs in terms of  $|\mathbf{E}|$ ,  $E_z$ ,  $E_y$  and  $B_x$  fields are shown, where a and y are the vertical and the horizontal axes. It is worthwhile to notice that the fields calculated by the two codes agree perfectly. Indeed, in Fig.3, the behavior of the normalized TTF is shown for the same cavities.

As for field normalization, it has been chosen to normalize the fields in such a way that the energy gain is 0.18 MeV, when the transit-time factor equals TTF ( $\beta_{opt}$ ) and  $\cos\phi=1$ .

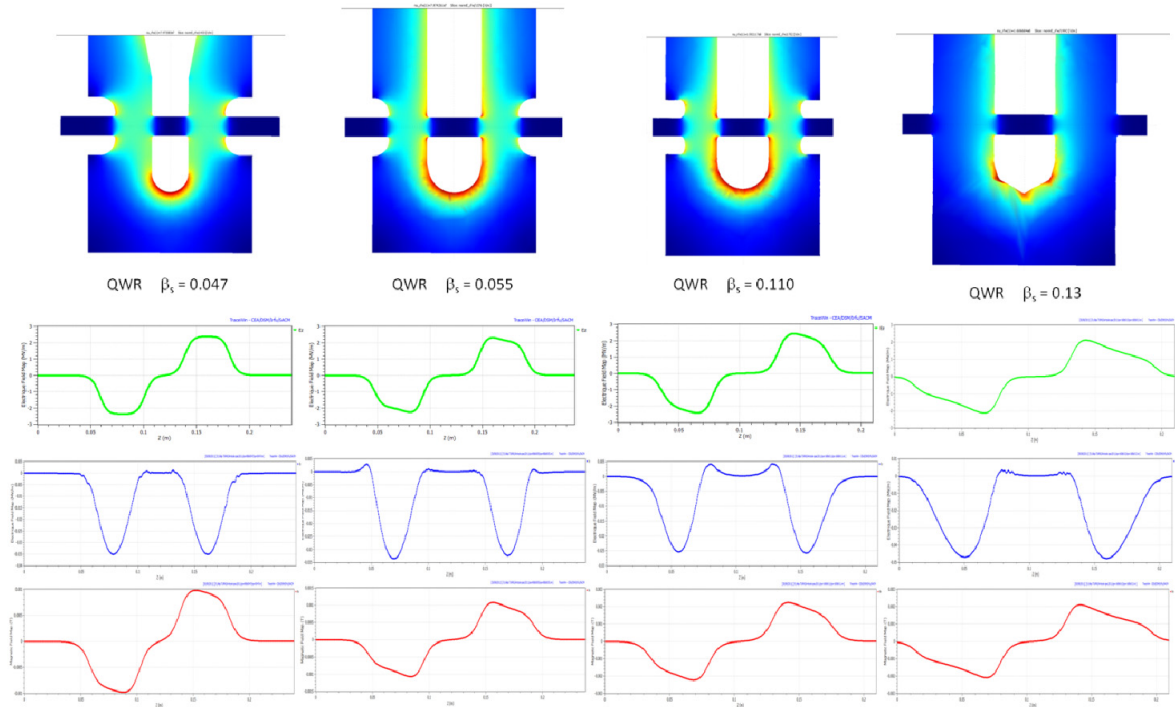


Figure 2: COMSOL simulation outputs for the first three families of cavities. From top to bottom: E field magnitudes (arbitrary units) on the vertical plane, E<sub>z</sub>, E<sub>y</sub> and B<sub>x</sub> components.

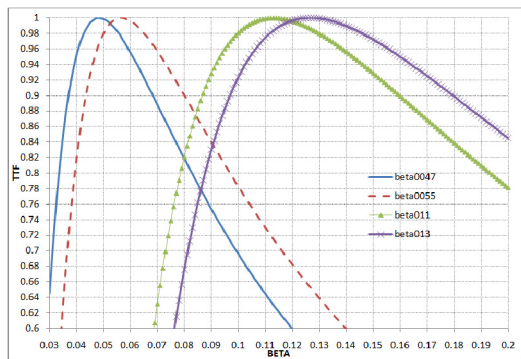


Figure 3: TTF(β)/TTF(β<sub>opt</sub>) for the four families of cavities.

### CALCULATION OF THE STEERING EFFECT

Another notable consequence of the simulation results is the calculation of the steering effect due to the on-axis fields of the cavities. In order to perform this calculation, the following relationship was used [1], which relates the longitudinal rate of change of the particle angle of deflection  $\alpha$  in the vertical plane, neglecting the change in particle velocity [2].

$$\frac{dy'}{dz} = \frac{qe}{Am_e c^2 \beta^2 \gamma} E_y(z) \cos\left(\frac{2\pi z}{\beta\lambda} + \varphi\right) + \beta c B_x(z) \sin\left(\frac{2\pi z}{\beta\lambda} + \varphi\right)$$

Where  $q$  is the ion charge state,  $A$  is the mass number,  $e$  is the elementary charge,  $m_e$  is the atomic unit mass,  $\gamma$  is the relativistic factor, and  $\lambda$  is the wavelength of the rf field

Upon integration along the cavity length one obtains the overall deflection angle one gets:

$$\Delta y'(\beta) = \int_{-l/2}^{l/2} \frac{d\alpha}{dz} dz \Big|_{\varphi=-20^\circ}$$

In the following graphs of figure 4 the values of deflection angles as a function of  $\beta$  are reported.

Since the output beta of the SC RFQ is equal to 0.0355, it is possible to notice that a significant beam deflection can occur once the beam passes through the QWR 0047 cavity type. The same problem is undergone by the QWR011 cavity type as they accelerate a beam injected by the TANDEM (typical output  $\beta=0.07$ ) [1].

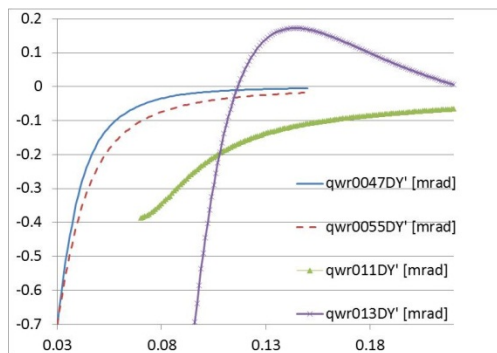


Figure 4: Deflection angle [mrad] as function of  $\beta$  for the four cavity families the species considered is proton and the synchronous phase is  $-20^\circ$ .

Another issue that was investigated was the effect of a beam displacement around the nominal position in terms of steering, in correspondence of the nominal beta value for all the cavity families. The results are shown in Figure 5.

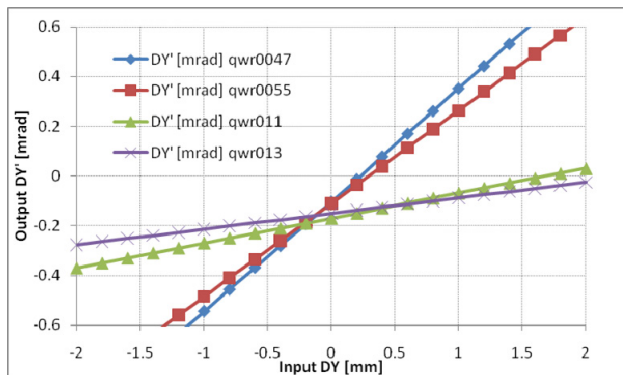


Figure 5: Deflection angle of the QWR cavities as a function of beam displacement.

From Figure 5, it can be assessed that, in order to avoid such deflection, it is necessary to inject the beam into the cavities slightly above the cavity axis, as also predicted in [3]. Moreover, it can be noticed that, although the QWR 0047 and QWR 0055 cavities undergo a higher deflection at the nominal beta when the beam crosses the cavity axis with respect to the other cavity families, they are as well less sensitive to beam position, as such steering effect is concerned.

### VERTICAL DISPERSION EFFECTS DUE TO BEAM STEERING

The last effect that was investigated is the derivative  $D'$  of the beam vertical dispersion due to magnetic field  $B_x$  only. The results are shown in Figure 6, in which the dispersion variation is mapped as a function of beta, under the same normalization used before.

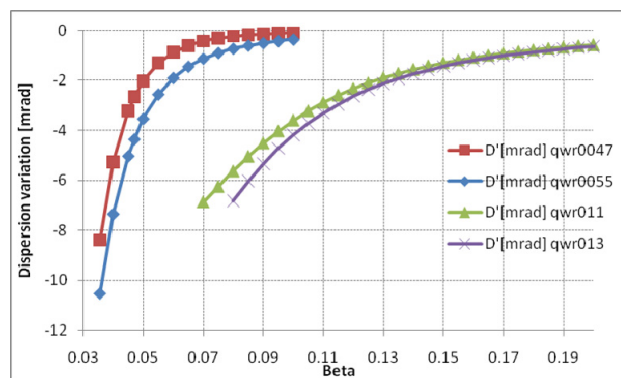


Figure 6: Dispersion variation as a function of  $\beta$  for the four cavity families.

From the above graph it results that the value of  $D'$  is significant when the beta is low. Due to the ALPI linac configuration, such cavity-induced dispersion is not compensated. This circumstance can induce beam losses and beam jitter as the beam itself is transported from the end of ALPI to the experimental halls.

### CONCLUSIONS

This investigation of the effect on beam transport based on the precise calculation of cavity fields highlighted some issues on beam behaviour, that were not evident with the usage of a thin-gap approach for the QWR ALPI cavities. Therefore a more precise beam correction scheme has become possible, which has led to an improvement of the overall machine setup in the last experimental shifts [1].

### REFERENCES

- [1] M. Comunian et al. these proceedings, WEPC014.
- [2] P. N. Ostroumov and K.W. Shepard, Phys. Rev. Spec. Top. Accel. And Beams 4 (2001) 110101.
- [3] A. Facco, V. Zviagintsev Phys. Rev. Spec. Top. Accel. And Beams 14 (2011) 070101.